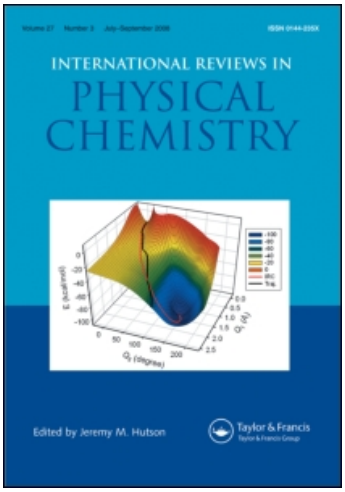

International Reviews in Physical Chemistry
Publication details, including instructions for authors and subscription information:
http://www.informaworld.com/smpp/title~content=t713724383

Dynamics of charge transfer and chemical reactions of doubly-charged ions at low collision energies

Zdenek Herman[a]
[a] J. Heyrovský Institute of Physical Chemistry, Academy of Sciences of the Czech Republic, Prague, Czech Republic

To cite this Article Herman, Zdenek(1996) 'Dynamics of charge transfer and chemical reactions of doubly-charged ions at low collision energies', International Reviews in Physical Chemistry, 15: 1, 299 — 324
To link to this Article: DOI: 10.1080/01442359609353186
URL: http://dx.doi.org/10.1080/01442359609353186

INTERNATIONAL REVIEWS IN PHYSICAL CHEMISTRY, 1996, VOL. 15, NO. 1, 299–324

Dynamics of charge transfer and chemical reactions of doubly-charged ions at low collision energies

by ZDENEK HERMAN

J. Heyrovský Institute of Physical Chemistry, Academy of Sciences of the Czech Republic, Dolejškova 3, CZ-18223 Prague 8, Czech Republic

Results of beam scattering studies on the dynamics of single charge transfer and chemical reactions of doubly-charged ions carried out in Prague are reviewed. Investigation of several atomic ion–atom charge transfer processes at collision energies 0·1–10 eV provides data on differential and relative total cross-sections of state-to-state processes. Populations of electronic and vibrational states of molecular product ions are obtained from experiments on molecular dication–atom and atomic ion (He^{2+})–molecule systems. Studies of chemical reactions of the dication CF_2^{2+} with D_2 show that Coulomb repulsion between the products ($CF_2D^+ + D^+$) governs the dynamics and energy partitioning.

1. Introduction

Investigation of the properties and reactivity of multiply-charged ions has become a very active field of research during the last fifteen years. In addition to being of fundamental importance, the studies indicate the important role these species are recognized to play in many areas such as astrophysics, laser research, thermonuclear fusion, material science etc. Besides atomic systems, molecular ions have also recently been investigated, in particular molecular dications. Valuable review articles have been published both on the atomic (Janev and Winter 1985) and molecular (Mathur 1993, Larsson 1993) ions.

The subject of this paper is a review of beam scattering studies of collision processes involving doubly-charged atomic and molecular ions carried out during the last decade at the J. Heyrovský Institute of Physical Chemistry in Prague. The studies concern only certain aspects of collision processes of dications, namely the dynamics of low energy (relative collision energy of about 0·1–10 eV) single-charge transfer processes and, in the most recent development, of chemical reactions of molecular dications. The main goal of these studies has been learning about the relative differential and total cross-sections of state-to-state processes. This required a combination of angular and product translational energy distribution measurements, as is typical in crossed-beam scattering experiments in the eV collision energy range.

Various types of processes have been investigated. In this paper experimental results concerning the following types of processes are discussed:

- atomic ion–atom charge transfer (differential cross-sections, relative total cross-sections of state-to-state processes);
- molecular ion–atom non-dissociative charge transfer (population of electronic and vibrational states of the product molecular ion);
- atomic ion–molecule non-dissociative charge transfer (population of vibrational states of the product molecular ion);
- chemical, bond-forming reactions of molecular dications.

Charge transfer processes of multiply-charged ions are characterized by exchange

0144–235X/96 $12·00

Table 1. Ionization energies of selected atoms and molecules

Atom Molecule	*IP*1 (eV) ($A \rightarrow A^+$)	*IP*2 (eV) ($A \rightarrow A^{2+}$)	ΔIP (eV) (*IP*2–*IP*1)
He	24·587	79·03	54·44
Ne	21·564	62·526	40·96
Ar	15·759	43·388	27·63
Kr	13·999	38·358	24·36
Xe	12·130	33·34	21·21
Hg	10·437	29·193	18·756
N_2	15·58	43·00	27·42
O_2	12·059	37·2	25·1
CO	14·013	41·29 (41·7)	27·3
NO	9·264	38·476	29·21
Cl_2	11·48	32·6	21·2
HCl	12·74	35·5	22·8
CO_2	13·769	37·4	23·6
N_2O	12·894	36·4	23·5
NH_3	10·166	33·7	22·6
C_6H_6	9·247	26·0	16·8

of a large amount of energy. In an electron capture process by a doubly-charged ion of the type

$$A^{2+} + B \rightarrow B^+ + B^+ \qquad (1)$$

(where A and B are atoms or molecules) basically the difference between the ionization energies of the dication and the respective cation A is available. Table 1 lists the ionization energies of ground state singly-charged and doubly-charged ions of a series of atoms and simple molecules, and the respective energy differences. It can be seen that these energy differences range from the huge 54·4 eV for He to about 20–25 eV for heavier rare gases and for most of the common molecules listed. This implies that the target particle can be not only ionized, but often also considerably excited. The fate of the energy transferred, whether deposited as translational, electronic or—in the case of molecules—vibrational (and rotational) energy was one of the questions addressed in our studies.

An attractive feature of processes (1) is the relative simplicity of the interaction potentials involved. The interaction between the reactants is determined primarily by the ion-induced dipole interaction between the dication and the neutral particle combined with repulsion at short internuclear separations; the interaction between the products by the Coulomb repulsion between two particles of the same charge. As a result, the interacting terms usually cross under an acute angle and the crossings are well localized. The Landau–Zener formalism can thus be successfully applied in most cases to describe the transition probability. From the applicability of the Landau–Zener approach a salient feature follows which governs the total cross-section of these processes; it is known as the 'reaction window' concept of the cross-section. One may view it qualitatively in the following way (figure 1, for an atomic ion–atom collision system): if the crossing between the reactant and product term occurs at very large internuclear separations, where the interaction is very small, the single-passage transition probability p is negligibly small and the colliding system remains on the incoming potential energy curve (case A, figure 1). If, on the other hand, the crossing occurs at small internuclear separations and the interaction is large, the reactant and

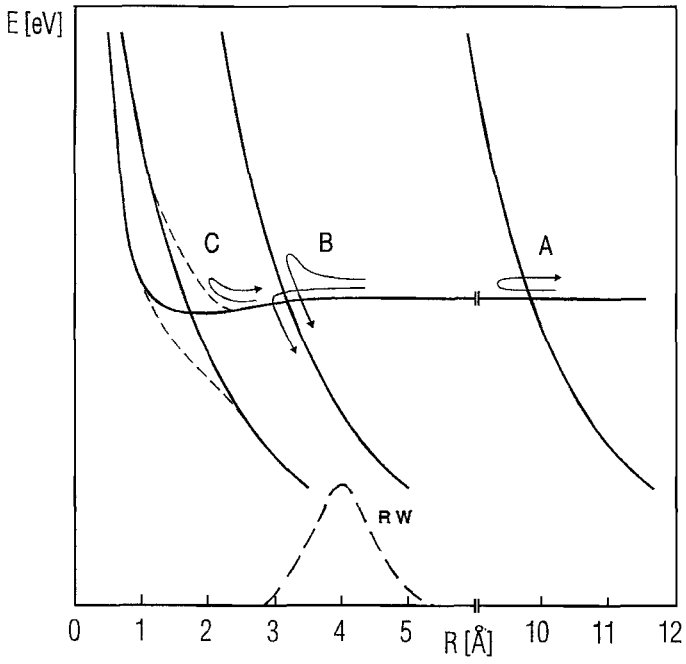

Figure 1. Schematics of potential energy curves for the reaction $A^{2+} + B \rightarrow A^{+} + B^{+}$. For details see text; only case (B) leads to charge transfer of a sizeable cross-section; RW = reaction window.

product terms split adiabatically and p is close to unity. The colliding system approaches and departs on the reactant potential energy curve, though at small interparticle separations it moves on the section of the potential energy curve which belongs to the products (C). Only if the crossing occurs within a certain range, where the single-passage transition probability is about 0·5 (say $0{\cdot}1 < p > 0{\cdot}9$), there is a finite chance that the system may approach on the reactant and depart on the product potential energy curve (B), and the cross-section of the charge transfer process is large. The overall transition probability includes the way in and out and is $P \simeq p(1-p)$. The position of the reaction window is determined by the Landau–Zener formula and for collision energies in the eV range it lies at about 2·5–5·5 Å (figure 1). The size of the total cross-section depends on the position of the crossing point, and it is thus related to the exoergicity of the process in question. The relation between the exoergicity ΔE and the position of the crossing point R_c may be roughly estimated (for a crossing of a flat and a Coulomb term) from

$$R_c = \frac{14{\cdot}4}{\Delta E} \tag{2}$$

where R_c is in Å, and ΔE in eV.

2. Experimental

Most of the experiments were carried out on the crossed beam scattering apparatus EVA II (figure 2). Briefly, reactant doubly-charged ions were produced by impact of 120–150 eV electrons on a suitable gas in a low pressure ion source. The ions were extracted, mass analysed, decelerated by a multielement electrostatic lens system to a desired laboratory energy in the eV region. The ion reactant beam had an energy

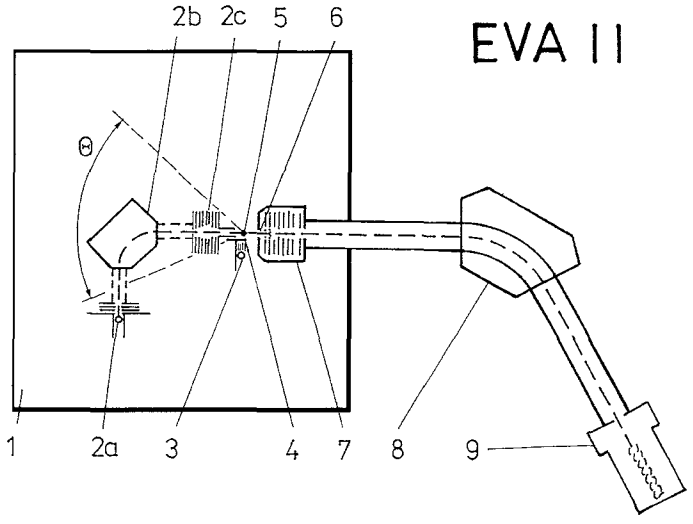

Figure 2. Crossed beam apparatus EVA II: 1 = scattering chamber; 2 = ion beam source: (a) electron impact ion source, (b) mass selecting magnet, (c) deceleration lens; 3 = neutral beam source; 4 = chopper; 5 = scattering zone; 6 = detection slit; 7 = energy analyser; 8 = detector mass spectrometer; 9 = multiplier.

spread of about 0·2–0·5 eV (FWHM, full width at half maximum) and an angular spread of about 1° (FWHM). The reactant beam was crossed at right angles by a collimated thermal beam of the neutral reactant emerging from a multichannel jet (angular spread of 10°, FWHM). The two beams rotated about the collision centre in the plane of the detector. Reactant and product ions were detected using a detection slit, energy analysed by a stopping-potential analyser, mass analysed, and registered by a multiplier. Modulation of the neutral reactant beam, phase sensitive detection, and signal averaging was used to deal with background problems. Raw data consisted of angular distributions and sets of energy profiles of reactant and product ions at a series of scattering angles. The data were used to construct contour scattering diagrams of the product ion. Further dynamical quantities (relative differential cross-sections, $P(\theta)$ versus θ, product relative translational energy distributions, $P(T')$ versus T'), were obtained by appropriate integration of the scattering diagrams (Friedrich and Herman 1984a).

Data on the He^{2+}–molecule charge transfer were obtained using the Göttingen crossed beam apparatus originally designed for high-resolution studies of inelastic scattering of protons (figure 3). The machine was adjusted to record the E–2E translational energy spectra and its overall resolution was about 120 meV; this was sufficient to resolve the vibrational structure in translational energy spectra of the molecular products investigated.

Translational energy spectra at keV projectile energies, briefly mentioned in the molecular dication–neutral atom charge transfer studies, were obtained with the use of the Swansea modified ZAB-2F mass spectrometer described elsewhere (Morgan *et al.* 1978). The resolution of the instrument at projectile energies of 6 keV was about 1 eV.

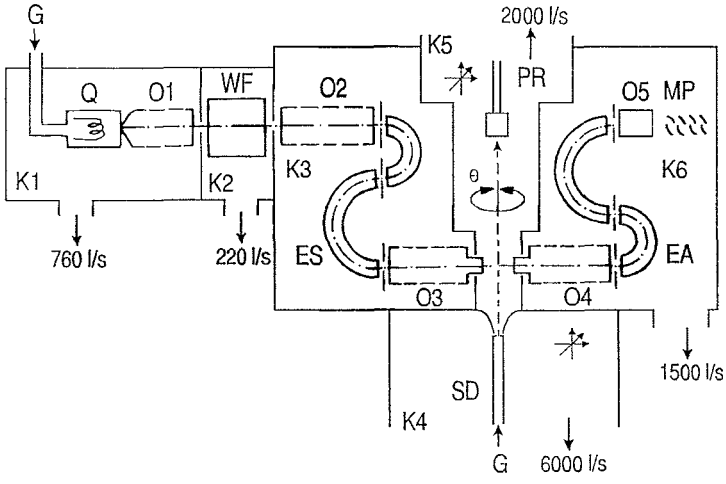

Figure 3. Göttingen scattering machine: Q = Colutron ion source; O1–O5 = ion optics systems; WF = Wien filter; ES = energy selector; SD = skimmed nozzle beam; EA = energy analyser; MP = electron multiplier; G = gas inlets; K1–K6 = differentially pumped chambers.

3. Results

3.1 *Atomic ion–atom systems*

3.1.1. $Ar^{2+} + He$

One of the first systems investigated in a crossed beam experiment (Friedrich and Herman 1984b) was the charge transfer process

$$Ar^{2+}(^3P, ^1D, ^1S) + He(^1S) \rightarrow Ar^+(^2P) + He^+(^2S). \tag{3}$$

The reactant beam of the dication formed by electron impact also contained, besides the ground state ^3P, metastable excited states ^1D and ^1S (we omit here references to fine structure states of the reactant and product ions which could not be resolved in the experiments). Thus there were three reactant entrance channels with exoergicities 3·00 eV, 4·74 eV and 7·12 eV, for Ar^{2+} in ^3P, ^1D and ^1S, respectively (figure 4). The scattering diagrams of the product Ar^+ at the collision energy $T = 0{\cdot}53$ eV is shown in figure 5: intensity ridges clearly indicate formation of products in reactions with Ar^{2+} in ^3P and ^1D, while the reaction with ^1S, too exoergic to fit into the reaction window at this collision energy, appears to make a negligible contribution. The scattering diagrams could be deconvoluted to provide data on the relative differential cross-section $P(\theta)$ (centre-of-mass angular distribution) of the state-to-state processes, figure 6. There is a pronounced difference in the shape of $P(\theta)$ for the ground state reactant $Ar^{2+}(^3P)$ and the metastable $Ar^{2+}(^1D)$. Can one understand the shape of the differential cross-section?

We developed a simple quasi-classical model (Friedrich *et al.* 1986) and calculated the differential cross-section for the state-to-state process

$$Ar^{2+}(^3P) + He(^1S) \rightarrow Ar^+(^2P) + He^+(^2S). \tag{4}$$

The two-level model assumed that the interaction potentials were determined (for the reactants) by the ion-induced dipole interaction combined with exponential repulsion at small internuclear separations, and (for the products) by Coulomb repulsion between two singly-charged ions. The analysis of the quasi-molecular terms showed that the leading interacting terms of the reactants and products were the $^3\Pi$ terms.

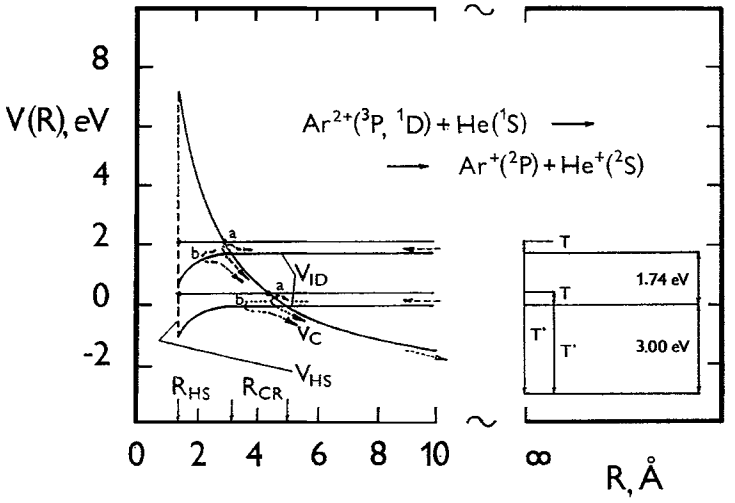

Figure 4. Potential energy curves for the charge transfer system $Ar^{2+} + He$: V_{ID}, V_C = interaction potentials; R_{CR} = crossing points; T′ = exoergicities of state-to-state processes (Friedrich and Herman 1984b).

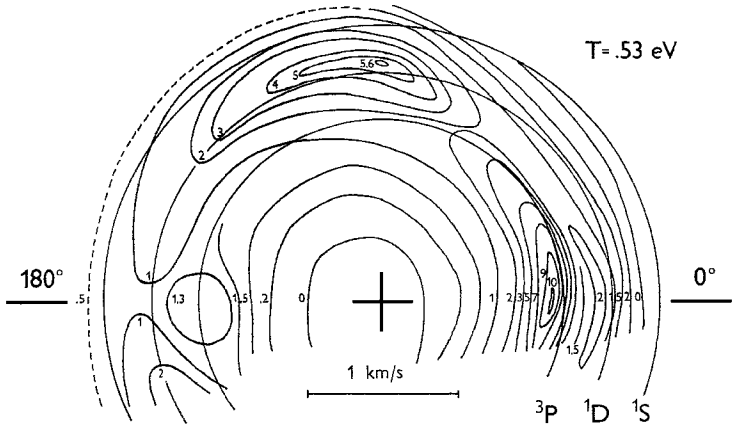

Figure 5. Contour scattering diagram of Ar^+ from reaction (3) at $T = 0{\cdot}53$ eV. Circles represent loci of c.m. velocities, as expected from exoergicities of processes with Ar^{2+} in ^3P, ^1D, ^1S states, respectively; cross marks the position of the tip of the c.m. velocity vector, relative velocity is directed along the 180°–0° axis (Friedrich and Herman 1984b).

Coupling of the diabatic terms was evaluated using the asymptotic method. The Landau–Zener model was used to calculate the respective transition probabilities assumed to be localized in the vicinity of the crossing points between the reactant and product potential terms. The potentials were used to calculate the classical deflection functions and from it the quasi-classical differential cross-section. The results, even for the simplest potentials, described correctly the shape of the differential cross-section (figure 7(*a*)).

In another theoretical study (Braga *et al.* 1986) of the charge transfer process (4), the two lowest $^3\Pi$ potential energy curves were calculated by the *ab initio* configuration interaction (CI) procedure using a large basis set, transformed to diabatic potentials, and the total and differential cross-section was determined using a quantum

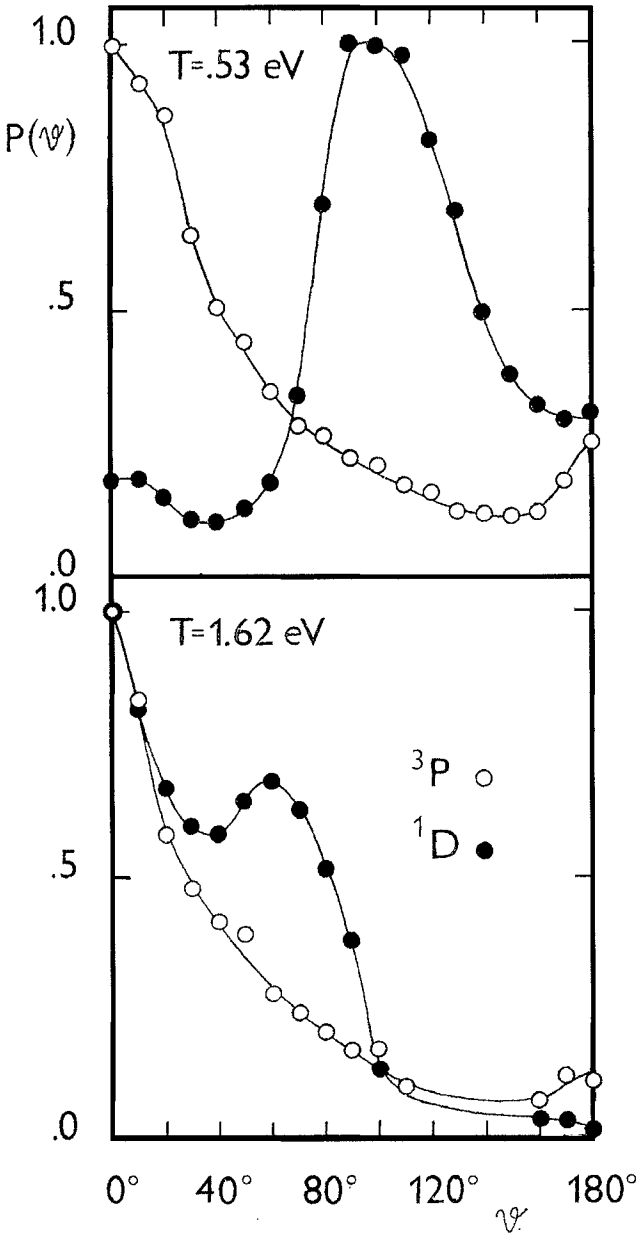

Figure 6. Relative differential cross-sections, $P(\theta)$ versus θ, of Ar^+ from reaction (3) for Ar^{2+} states ^3P and ^1D at $T = 0{\cdot}52$ eV and $T = 1{\cdot}62$ eV (Friedrich and Herman 1984b).

mechanical close coupling calculation. The differential cross-section was then compared with the above mentioned experimental results (Friedrich and Herman 1984b), after being averaged over the centre-of-mass (c.m.) angular resolution of the experiment, $\Delta\theta = 12°$. The agreement was good (figure 7(*b*)). The quantum mechanical calculations also led to a fair agreement with the experimental values of the total cross-section.

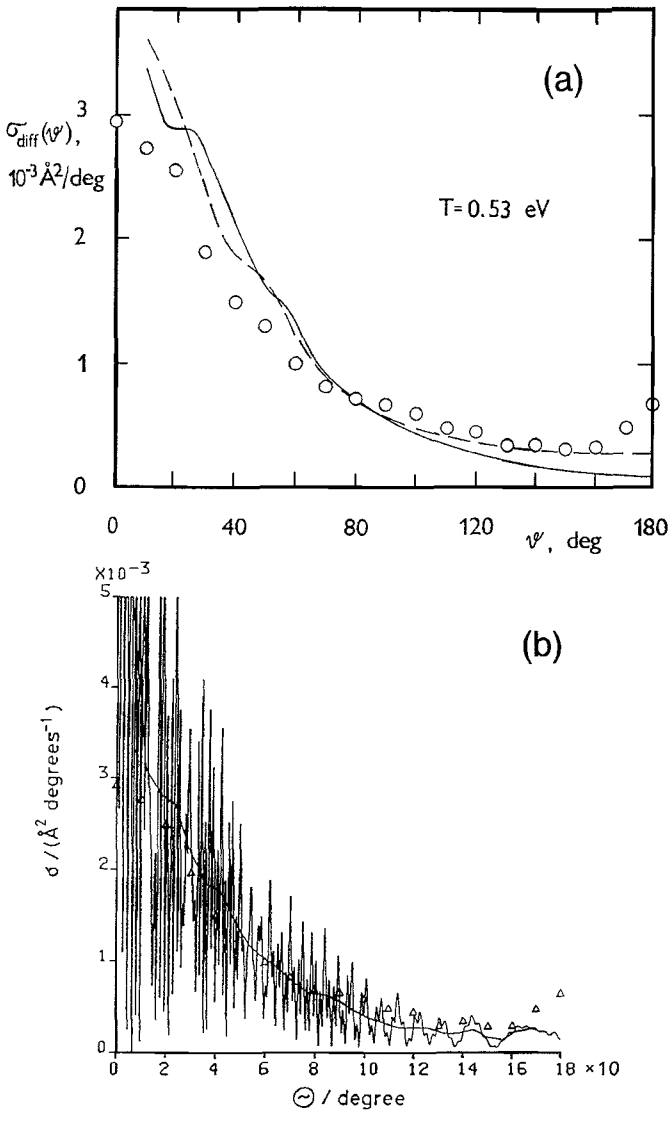

Figure 7. Relative differential cross-sections of Ar^+ from reaction (4), $Ar^{2+}(^3P)+He$: comparison of experimental (o, △) (Friedrich and Herman 1984b) and theoretical results as obtained from (*a*) quasi-classical model (Friedrich *et al.* 1986) and (*b*) quantum mechanical calculations (Braga *et al.* 1986).

3.1.2. $Kr^{2+}+He$

In the previous experiments, the spin–orbit states of the product ion could not be resolved. In order to obtain information on the relative differential and total cross-sections for the formation of the spin–orbit states in a charge transfer process which involves a rare gas dication, the single-charge transfer reaction

$$Kr^{2+}(^3P, ^1D, ^1S)+He(^1S_0) \rightarrow Kr^+(^2P_{3/2,1/2})+He^+(^2S_{1/2}) \qquad (5)$$

was studied in a crossed beam experiment (Friedrich *et al.* 1987). The energy difference between the two spin–orbit states of Kr^+ is 0·66 eV and this difference could be

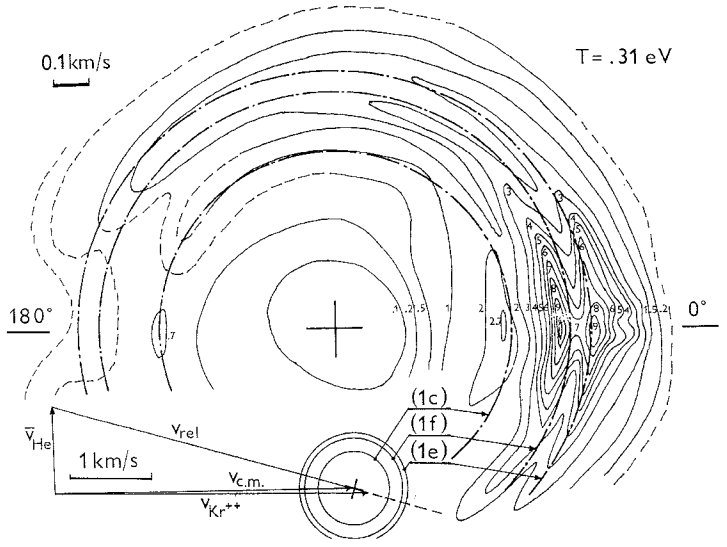

Figure 8. Contour scattering diagram of Kr^+ from reaction (5) at $T = 0{\cdot}31$ eV. Concentric circles show loci of product ion c.m. velocities from reactions: $Kr^{2+}(^1S) + He$ to $Kr^+(^2P_{3/2})$ (1c) and to $Kr^+(^2P_{1/2})$ (1f); and of $Kr^{2+}(^1D) + He$ to $Kr^+(^2P_{3/2})$ (1c). Inset: Newton diagram of the process (Friedrich *et al.* 1987).

resolved in the present experiments. Figure 8 shows a contour scattering diagram of Kr^+ at $T = 0{\cdot}31$ eV. In this system, reactions of the ^3P states of Kr^{2+} are endoergic and those of the ^1D state exoergic by only 1·13–1·79 eV. The main ridges in the contour diagram correspond, therefore, to processes of $Kr^{2+}(^1S)$ leading to $Kr^+(^2P_{3/2})$ ($\Delta E =$ 4·07 eV; reaction (1e) in figure 8) and $Kr^+(^2P_{1/2})$ ($\Delta E = 3{\cdot}42$ eV; reaction (1f)); the inner ridge is due to $Kr^{2+}(^1D) \rightarrow Kr^+(^2P_{3/2})$ ($\Delta E = 1{\cdot}79$ eV; reaction (1c)). By integrating the scattering diagrams the relative product translational energy distribution, $P(T')$, was obtained (figure 9) and by its deconvolution the relative ratios of the total cross-sections for the respective state-to-state processes, assuming that the abundance of the reactant electronic states in the beam was statistical, as confirmed by other measurements (Kobayashi *et al.* 1983).

Processes (1e) and (1f) (in figure 8) have about the same cross-section, whilst the cross-section of process (1c) is about 10% of the sum of (1e) and (1f). The results are in good agreement with total cross-section measurements and calculations of Okuno and Kaneko (1983). The shape of the differential cross-sections was in general agreement with the predictions of the above mentioned quasi-classical model.

3.1.3. *$Hg^{2+} + Kr(Ar)$*

The question of population of spin–orbit states was further investigated in studies of the system (Friedrich *et al.* 1985)

$$Hg^{2+}(^1S) + Kr(^1S) \rightarrow Hg^+(^2S) + Kr^+(^2P_{3/2,\,1/2}). \tag{6}$$

The reaction leading to the (3/2) state is exoergic by 4·77 eV, that leading to the (1/2) by 4·12 eV. The scattering experiments were carried out over the collision energy range 0·9–2·7 eV. The scattering diagrams, differential cross-sections (which could be well described by the quasi-classical model) and relative product translational energy distributions showed that the total cross-section ratio $\sigma(3/2)/\sigma(1/2)$ was slightly

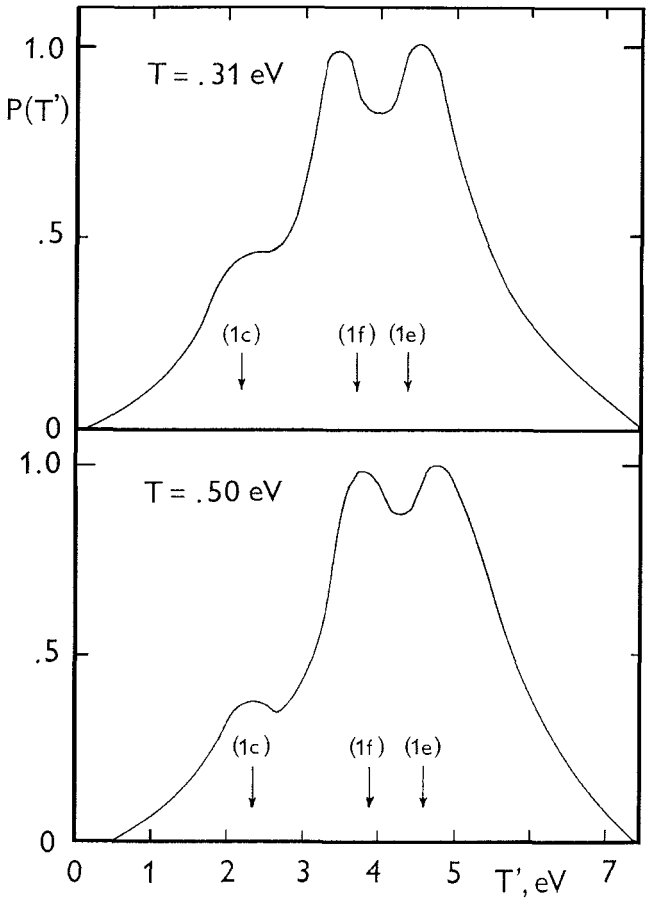

Figure 9. Relative translational energy distributions, $P(T')$, of reaction products of Kr^{2+} + He charge transfer at collision energies of 0·31 eV and 0·5 eV; (1c)–(1f) refer to state-to-state processes from figure 8 (Friedrich *et al.* 1987).

greater than 1·0 at low collision energies, and at $T = 2{\cdot}71$ eV it approached the value 0·8; this value was close to the ratio of the maximum impact parameters $b^2_{max}(3/2)/b^2_{max}(1/2)$, where b_{max} was related to the respective crossing radius (Friedrich *et al.* 1986).

The beam of Hg^{2+} formed by electron impact is known to also contain, besides the ground state ions $Hg^{2+}(^1S)$, ions in the excited metastable state $Hg^{2+}(^3D_{3,2,1})$. The reactivity of these excited states was clearly demonstrated in charge transfer reactions of Hg^{2+} with Ar and Kr, both by the results of beam scattering and selected-ion flow drift tube experiments (Hansel *et al.* 1992). The reason why the metastable $Hg^{2+}(^3D)$ states did not play a significant role in reactions with Kr was found in the core-conservation rule, known to operate well at high (keV) collision energies (Janev and Winter 1985 and references cited therein). According to this rule, these processes tend to have large cross-sections which occur through a simple electron capture and do not require a reorganization of the core electrons of the projectile. On the other hand, processes which need a core electron reorganization tend to have small cross-sections. In our case, there is a series of reactions between $Hg^{2+}(^3D_j)$ and Kr which could lead to excited states of the Hg^+ product (^2D_j, ^2P_j) in processes of similar exoergicities as

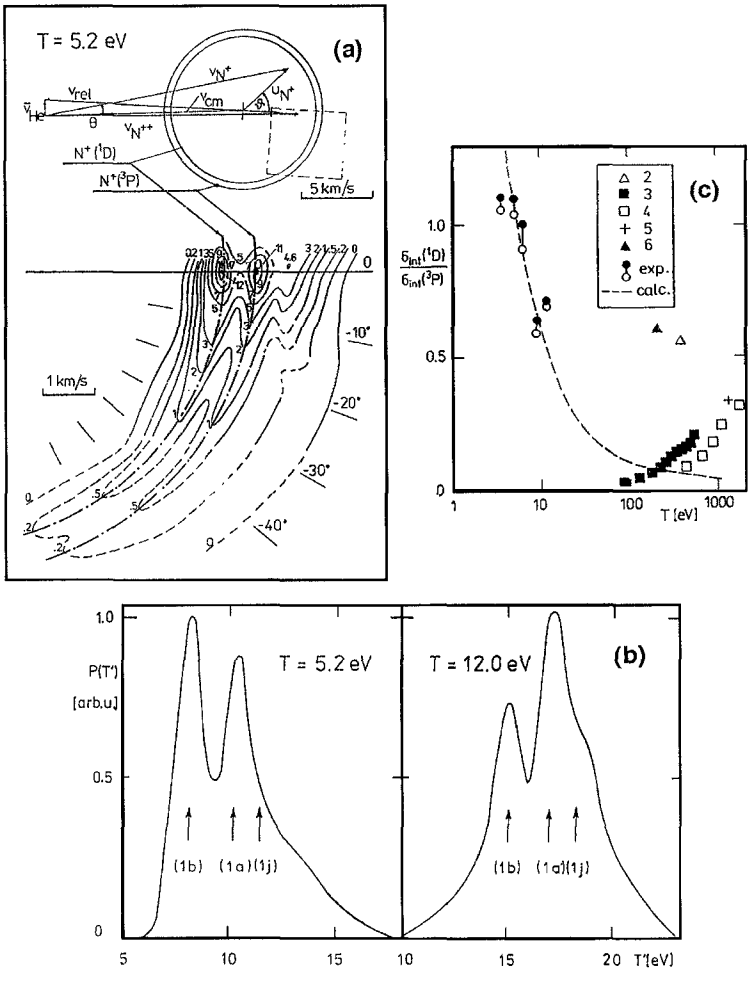

Figure 10. Formation of N^+ in reaction (7): (*a*) Newton diagram and contour scattering diagram at $T = 5{\cdot}2$ eV; (*b*) product relative translational energy distributions, $P(T')$, at $T = 5{\cdot}2$ eV and $T = 12{\cdot}0$ eV, arrows correspond to formation of $N^+(^3P)$ (1a), $N^+(D)$ (1b) and side reactions of $N^{2+}(^4P)$ admixtures (1j); (*c*) dependence of $\sigma(^1D)/\sigma(^3P)$ on collision energy T, solid and open circles are our low energy data, high energy data are from various sources, dotted line = semiempirical calculations (Sadílek *et al.* 1990).

reaction (6), and which should effectively compete with (6). However, most of them do not conserve the core of the Hg ions and thus the state-to-state processes (6) prevail (Hansel *et al.* 1992). These conclusions indicated that the core-conservation rule, known to operate at medium and high collision energies, was also valid at eV and sub-eV energies and should be taken into account when analysing charge transfer data in this energy region.

3.1.4. $N^{2+} + He$

The reaction

$$N^{2+}(^2P) + He(^1S) \rightarrow N^+(^3P, ^1D) + He^+(^2S) \qquad (7)$$

is of astrophysical interest, because of its possible importance in cold plasma nova

shells as a source of metastable $N^+(^1D)$. Experimental data available only at keV collision energies revealed preferential formation of the ground state $N^+(^3P)$ ($\Delta E = 5{\cdot}02$ eV). Theoretical calculations (Dalgarno 1985) for low collision energies suggested, however, preferential formation of the excited ^1D state ($\Delta E = 3{\cdot}12$ eV). Experimental data on reaction (7) at low collision energies were therefore needed.

In our study, reaction (7) was investigated in the collision energy range 3·8–12 eV (Sadílek *et al.* 1990). The scattering diagrams (figure 10(*a*)) show two ridges corresponding to exoergicities of the two above mentioned processes. From the scattering diagrams $P(T')$ versus T' dependences were derived (Figure 10(*b*)) and by integrating the intensity under the curves the ratio of the total cross-sections for the formation of the two states, $\sigma(^1D)/\sigma(^3P)$, could be evaluated. The ratio of the cross-sections was found to increase rather sharply from 0·5 to about unity below 10 eV (c.m.). Figure 10(*c*) summarizes the data together with the high energy data from various other sources, mostly from Sato and Moore (1979) and Lennon *et al.* (1983). The dashed curve in figure 10(*c*) represents results of our semiempirical calculation based on the Landau-Zener model (Olson 1972). Recent high-quality calculations (Dalgarno 1993) stress important contributions to the total cross-section of Demkov-type transitions in areas different from the vicinity of the potential term crossing points, and conclude that the cross-section ratio increases sharply at somewhat lower energies (about 1 eV) than observed by us.

3.2 *Molecular ion–atom systems*

Low energy scattering studies were preceded by a general mapping study of several molecular ion–atom systems at energies of the projectile ion 6 keV, using the Swansea mass spectrometric techniques. Translational spectra recorded in the direction of the projectile ion movement were obtained with a resolution of about 1 eV. One of the systems studied was CO^{2+} with rare gases (Herman *et al.* 1987). Translational energy spectra of CO^+ formed in collisions of CO^{2+} with Ne and Ar are shown in figure 11. Little was known about the non-dissociating electronic states of CO^{2+} at the time of the study, and there was a considerable scatter of data even on the lowest ionization potential of the projectile dication. Our translational spectroscopy results were consistent with the lowest ionization potential of a non-dissociative state $IP(CO \rightarrow CO^{2+}) = 41{\cdot}0$ eV; this value is in fair agreement with the very recent value of 41·29 eV (Dawber *et al.* 1994).

The translational energy spectra in figure 11 (scales Iα-) fit fairly well the exoergicities of transitions to the ground and excited states of the product CO^+. In addition, they show a considerable broadening of the peaks which suggests population of a series of vibrational levels within a given electronic state. The resolution of the experiment did not allow, unfortunately, for a more detailed analysis of the spectra. One should note here that the position of the CO^{2+} excited state in our data (scale IIα- in figure 11) was erroneously ascribed and should be entirely disregarded. The highest peaks in the spectra correspond well to the reaction window concept: in charge transfer with Ne the molecular product CO^+ was formed with largest probability in the ground $X^2\Sigma^+$ state (peak of the reaction window calculated at $\Delta E = 5{\cdot}3$ eV), in reaction with Ar the $CO^+(B^2\Sigma^+)$ state was most likely formed (reaction window peak at 4·4 eV).

In the next few years two important pieces of information became available on this system. Larsson *et al.* (1989) published an advanced theoretical treatment of the potential energy curves of CO^{2+}. The study concluded that the two lowest non-

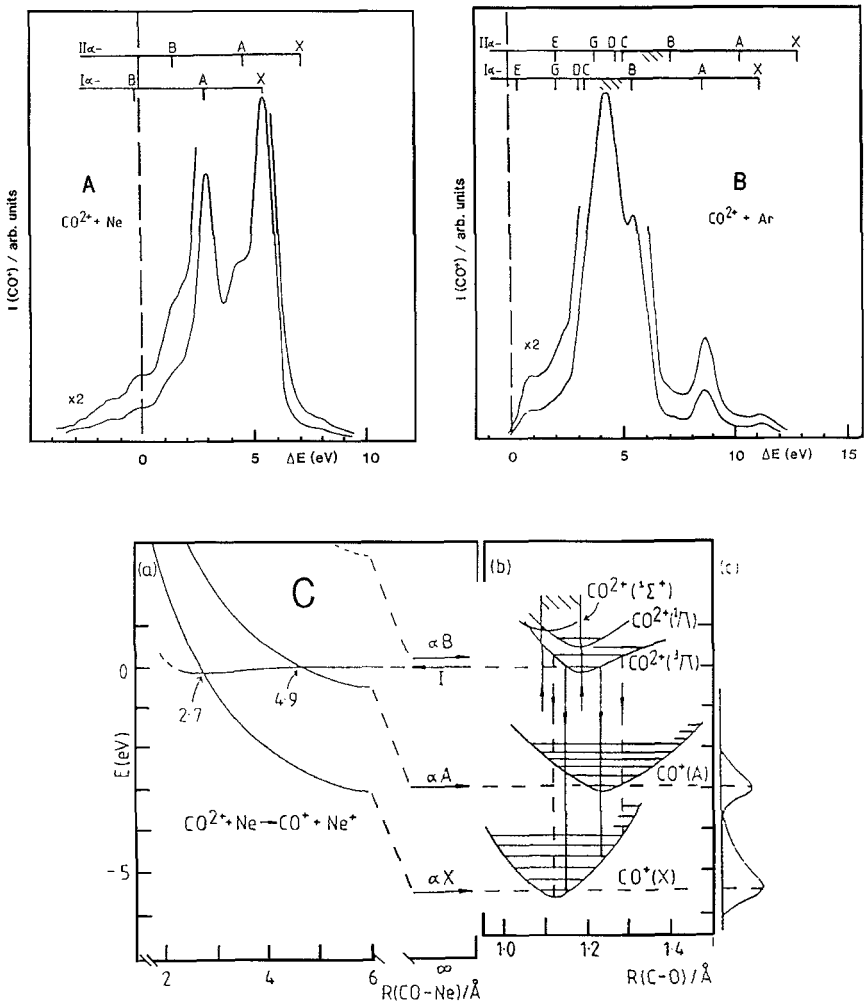

Figure 11. Translational energy spectra of CO^+ from reaction of 6 keV CO^{2+} with Ne(A) and Ar(B) plotted against the reaction exoergicity ΔE. (C) schematics of potential energy surfaces for CO^{2+} + Ne: (a) along the CO–Ne interparticle axis at a fixed C–O distance; (b) along the C–O internuclear axis at infinite separations between reactants; (c) schematics of expected translational energy spectrum (Herman *et al.* 1987).

dissociative states of CO^{2+} were the $1^3\Pi$ state (ground state) and the $1^1\Sigma^+$ state, lying just 0·25 eV above the ground state. All other states of the triplet and singlet progressions came out as dissociative or predissociative. The calculations also provided spectroscopic data on the lifetimes of the vibrational states. From a thorough discussion it followed that only ground vibrational states of the $1^3\Pi$ and $1^1\Sigma^+$ should have lifetimes of 10^{-5} s or longer.

The other piece of information came from a beautiful experiment carried out in Swansea: using a new spectrometer, Hamdan and Brenton (1989) could resolve in the translational energy spectrum of the system CO^{2+} (6 keV) + Ne electronic *and* vibrational states of the CO^+ product. Unfortunately, the peaks were only formally assigned to a vibrational progression of one electronic state, though changes in their intensities indicated a more complicated situation.

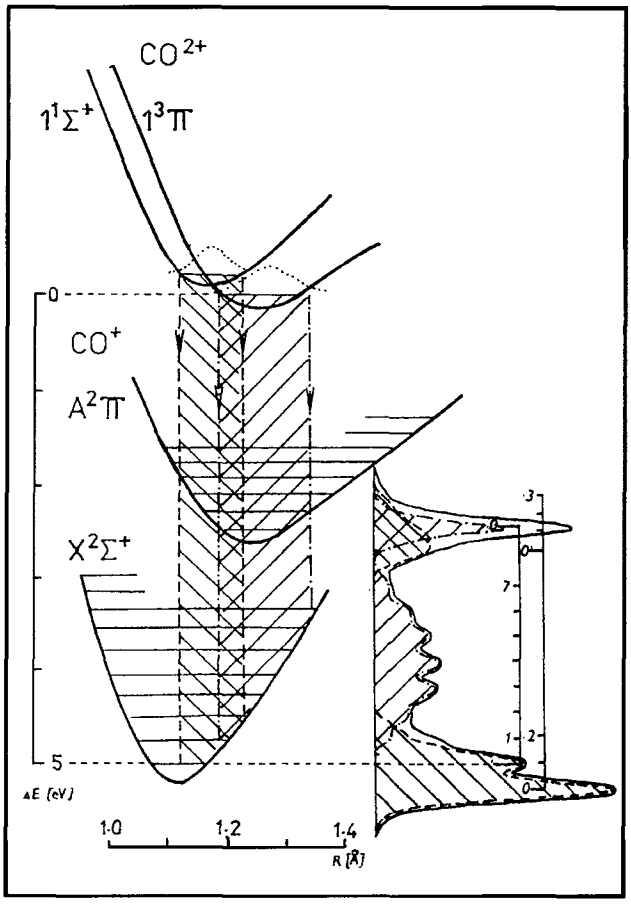

Figure 12. Summary of the analysis of CO^{2+} (6 keV) + Ne translational energy spectrum: left = potential energy curves involved and regions of vertical transitions; right = spectrum construction from particular state-to-state contributions (Fárník 1991).

As a part of our low energy scattering study of the system $CO^{2+} + Ne$, we analysed the well-resolved spectrum of Hamdan and Brenton in terms of the potential energy curves calculated by Larsson *et al.* (1989). At the projectile energy of 6 keV the collision time is much shorter than a typical vibrational period, and one may regard the vibration of the molecular species as frozen during the collision. This simplifies the picture and makes it possible to analyse the process in terms of vertical transitions between potential energy curves of the system. The summary of the analysis is shown in figure 12 from the point of view of the internuclear axis C–O (Fárník 1991, Fárník and Herman 1991). There are two molecular reactant states assumed to be only in their vibrationally ground states and two product molecular states. Therefore, four different transitions between the molecular species contribute to the translational energy spectrum

$$CO^{2+}(1^3\Pi, 1^1\Sigma^+) + Ne(^1S_0) \rightarrow CO^+(X^2\Sigma^+, A^2\Pi) + Ne^+(^2P_{3/2,1/2}). \quad (8)$$

The product Ne^+ was assumed to be formed in the respective spin–orbit states in the statistical ratio. The relative weights of the particular transitions W (in fact, products

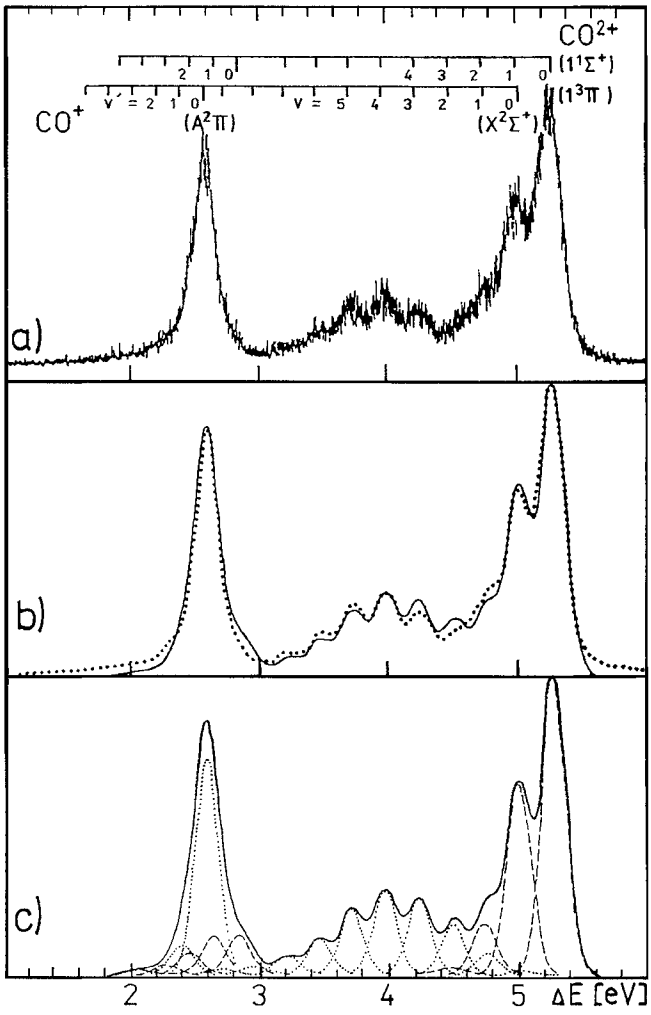

Figure 13. Analysis of the high-resolution translational energy spectrum of CO^+ from collisions of 6 keV CO^{2+} with Ne, reaction (8): (*a*) experiment of Hamdan and Brenton (1989), scales show positions of reactant and product states plotted against reaction exoergicity ΔE; (*b*) spectrum simulation: solid line = calculated fit (Fárník 1991), dotted line = experimental spectrum from (*a*); (*c*) details of the calculated fit, particular state-to-state contributions.

of the electronic transition probability and of the relative (unknown) concentration of the reactant electronic state in the beam at the scattering centre) were tentatively varied to achieve the best fit with the spectrum. The agreement between calculated and experimental data was very good (figure 13) and it was obtained with the relative weights of the transitions $W(^3\Pi \rightarrow X^2\Sigma) = 0{\cdot}65$, $W(^3\Pi \rightarrow A^2\Pi) = 0{\cdot}4$, $W(^1\Sigma \rightarrow A^2\Pi) = 0{\cdot}3$ and $W(^1\Sigma \rightarrow X^2\Sigma) = 1{\cdot}0$. This agreement confirmed the results of the calculations of the potential energy curves of CO^{2+} by Larsson *et al.* (1989); it was consistent both with the energy separation of the minima (0·25 eV) and with the equilibrium distances calculated for the $1^3\Pi$ and $1^1\Sigma^+$ state.

A scattering experiment on the reaction $CO^{2+} + Ne$ at eV collision energies was then carried out (Fárník 1991, Fárník and Herman 1991). The scattering diagram of

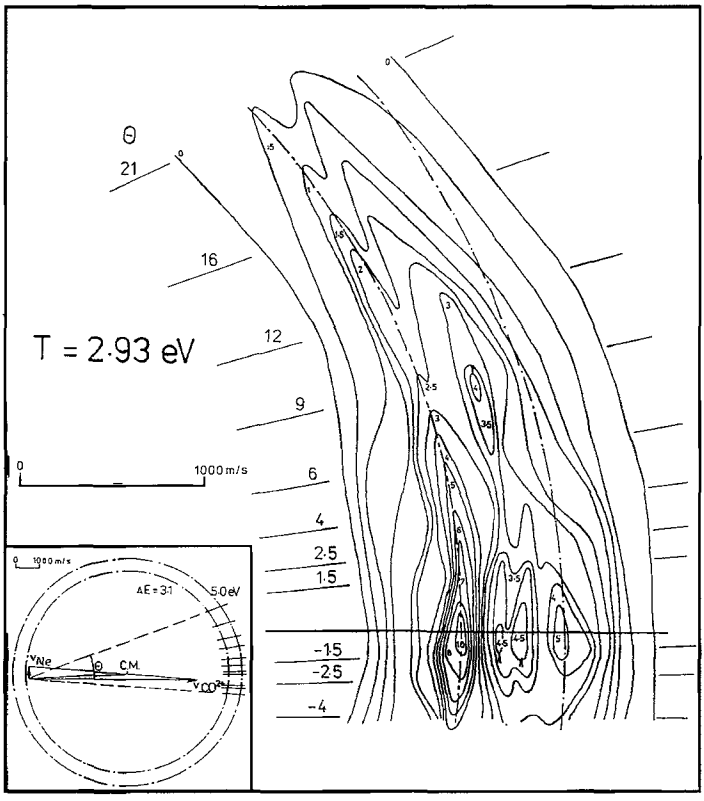

Figure 14. Contour scattering diagram of CO^+ from low energy collisions of CO^{2+} (7·0 eV) with Ne ($T = 2{\cdot}93$ eV); inset shows the respective Newton diagram.

the CO^+ product at the projectile energy of 7·0 eV (more than 10^3 times lower than in the experiment by Hamdan and Brenton (1989); $T = 2{\cdot}93$ eV) is shown in figure 14. Figure 15 illustrates the translational energy profile at the scattering angle $\theta_{LAB} = -1{\cdot}5°$ (angular maximum). The resolution of the experiment was about 0·3 eV and thus the vibrational states were not fully resolved; only a partly resolved vibrational envelope was obtained. Nevertheless, a comparison of the translational energy spectra in figures 13 and 15 shows that by changing the collision energy the population of both electronic and vibrational states of the molecular product CO^+ from reaction (8) changed considerably. This was evidently due to the change in the collision time: while at the projectile energy of 6 keV the effective collision time is only a fraction of a characteristic vibrational period, at 7 eV the molecular species may vibrate several times during the collision. As a result, at low collision energies the system reflects the shape of the potential energy surfaces in the interaction region, and the influence of the interaction between the reactants and products on the transition probabilities over the region where the surfaces cross. It is interesting to note that the low energy translational energy spectrum could be tentatively modelled assuming that the interaction between the reactants loosened up the CO^{2+} bond length slightly (by 0·03 Å for $^3\Pi$ and 0·04 Å for $^1\Sigma^+$ state, see figure 16). The simulation of the low energy spectrum shown in figures 15 and 16 was carried out in an analogous way as in the above mentioned high energy case (figure 13).

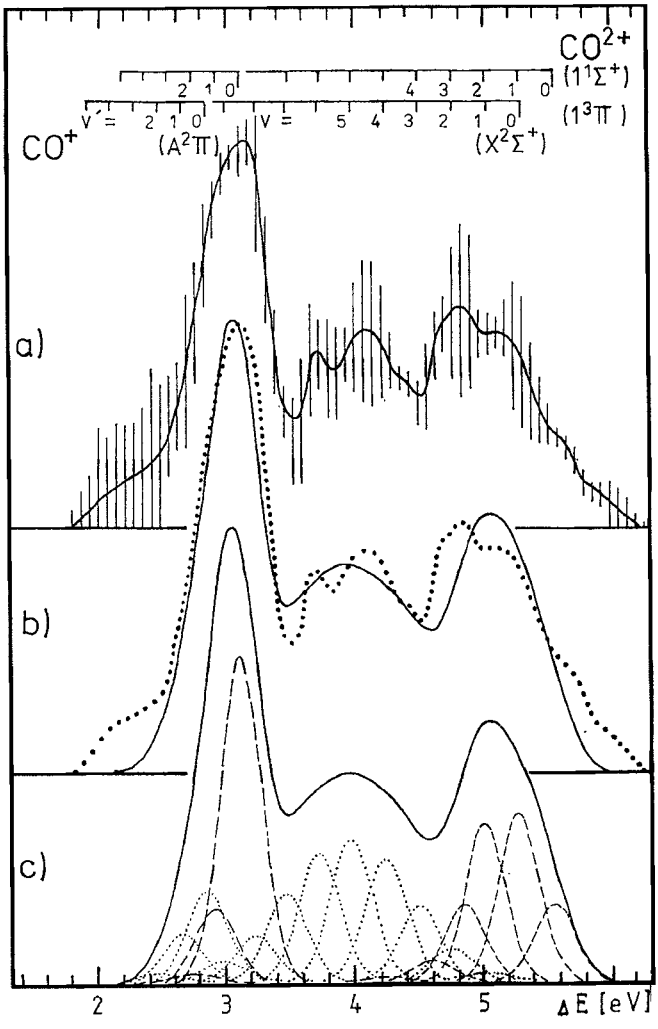

Figure 15. Translational energy spectrum of CO^+ from CO^{2+} (7·0 eV) + Ne plotted against the reaction exoergicity ΔE: (*a*) experiment at $\theta_{LAB} = -1{\cdot}5°$; (*b*) simulation: solid curve = calculated fit, dotted = experiment; (*c*) details of simulation with particular state-to-state contributions (Fárník 1991).

The charge transfer system CO^{2+} + Ne provided an example of a system in which interaction between the reactants and/or between the products led to a considerable perturbation of the potential energy surfaces. This was reflected in differences of the population of electronic and vibrational states of the product CO^+ at high and low collision energies. These model considerations appear to be supported by results of preliminary calculations on the changes of the $(C{-}O)^{2+}$ bond length upon Ne atom approach.

3.3. *Atomic ion–molecule systems*

In charge transfer collisions which involve molecular targets the energy available may be deposited not only into the translational and electronic energy of the products, but also into the internal (vibrational and rotational) degrees of freedom of the molecular product(s). Though translational energy spectroscopy studies on charge

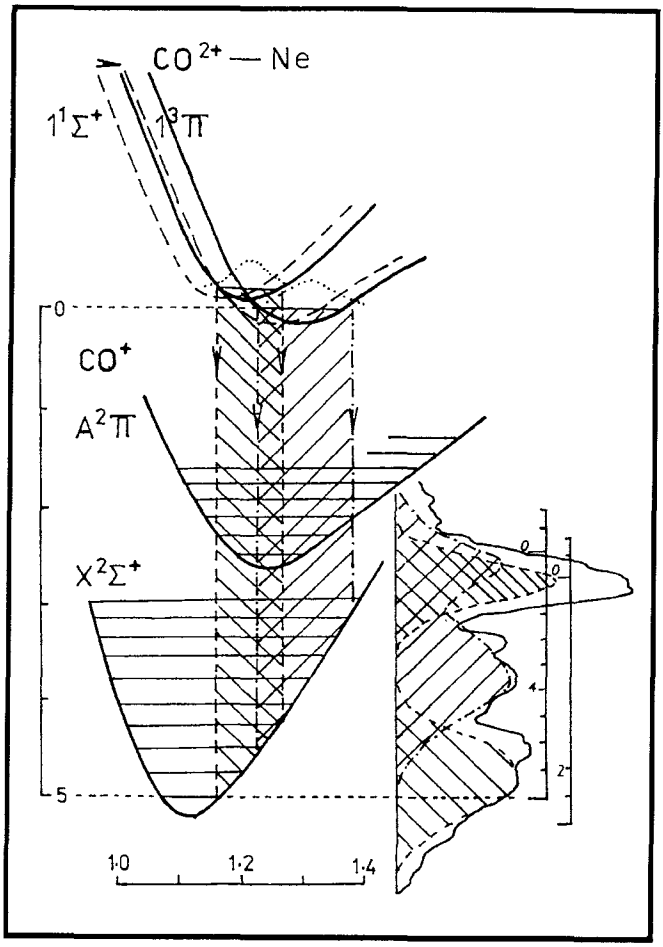

Figure 16. Summary of the analysis of low energy CO^{2+} (7·0 eV) + Ne translational energy spectrum in figure 15: left = potential energy curves (dotted curve = unperturbed, solid curve = shifted to reproduce the data) and regions of transitions; right = spectrum construction from state-to-state contributions (Fárník 1991).

transfer with atomic projectile ions, especially at keV energies, sometimes included molecular targets (H_2, N_2, O_2), there has been little information on the population of vibrational states of the molecular species formed. In addition, the problem may be complicated by dissociative processes. Addressing the problem of the vibrational state population thus requires high-resolution studies and the choice of a suitable system in which the dissociative processes do not occur.

We have found a class of processes which are suitable for such studies in charge transfer collisions between He^{2+}(IP = 79·00 eV) and molecules of an ionization potential of 9–10 eV (Fárník *et al.* 1993, 1995): in this case the reaction window concept may favour the formation of the excited He^{+}*(^{2}P) product (IP = 65·4 eV) and the ground state molecular ion (about 3 eV is assumed to go into the relative translational energy of the two positively-charged product ions)

$$He^{2+} + M \rightarrow He^{+}*(^2P) + M^{+}(v^{+}) \qquad (9)$$

(v^{+} refers to the vibrational state of the ion).

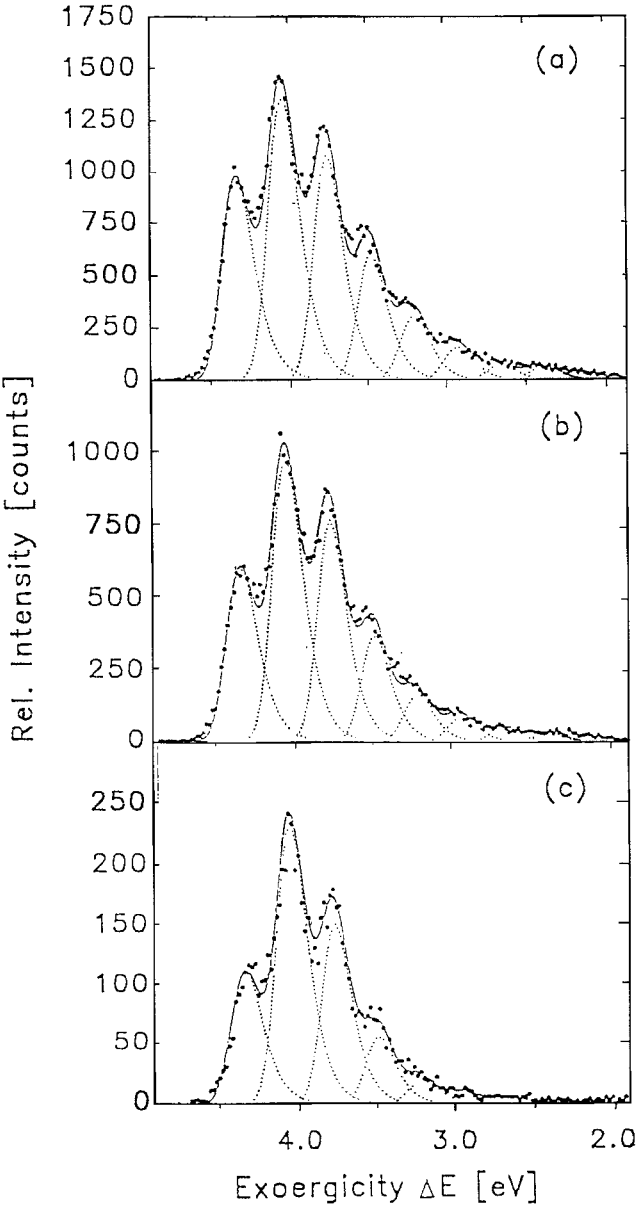

Figure 17. Translational energy spectrum of NO^+ from reaction (10) at the laboratory scattering angles (*a*) 0·0°, (*b*) 1·0°, (*c*) 2·5°; laboratory energy scale converted to reaction exoergicity ΔE, solid curve is the sum of peaks resulting from a computer fit (Fárník *et al.* 1993).

We applied this approach successfully to the investigation of the vibrational state populations of $NO^+(^1\Sigma^+)$, $NH_3^+(^2A_1)$ and $H_2S^+(^2B_1)$ formed in collisions of 70 eV He^{2+} with the respective molecules. The Göttingen crossed beam scattering machine was used in these experiments; the energy spread of the reactant ion beam was about 40 meV charge^{-1} and the overall resolution of the machine was about 120 meV.

The translational energy spectra of He^+ from charge transfer process

$$He^{2+} + NO(^2\Pi) \rightarrow He^{+*}(^2P) + NO^+(^1\Sigma^+, v^+) \quad (\Delta E_{v=0} = 4{\cdot}34 \text{ eV}) \qquad (10)$$

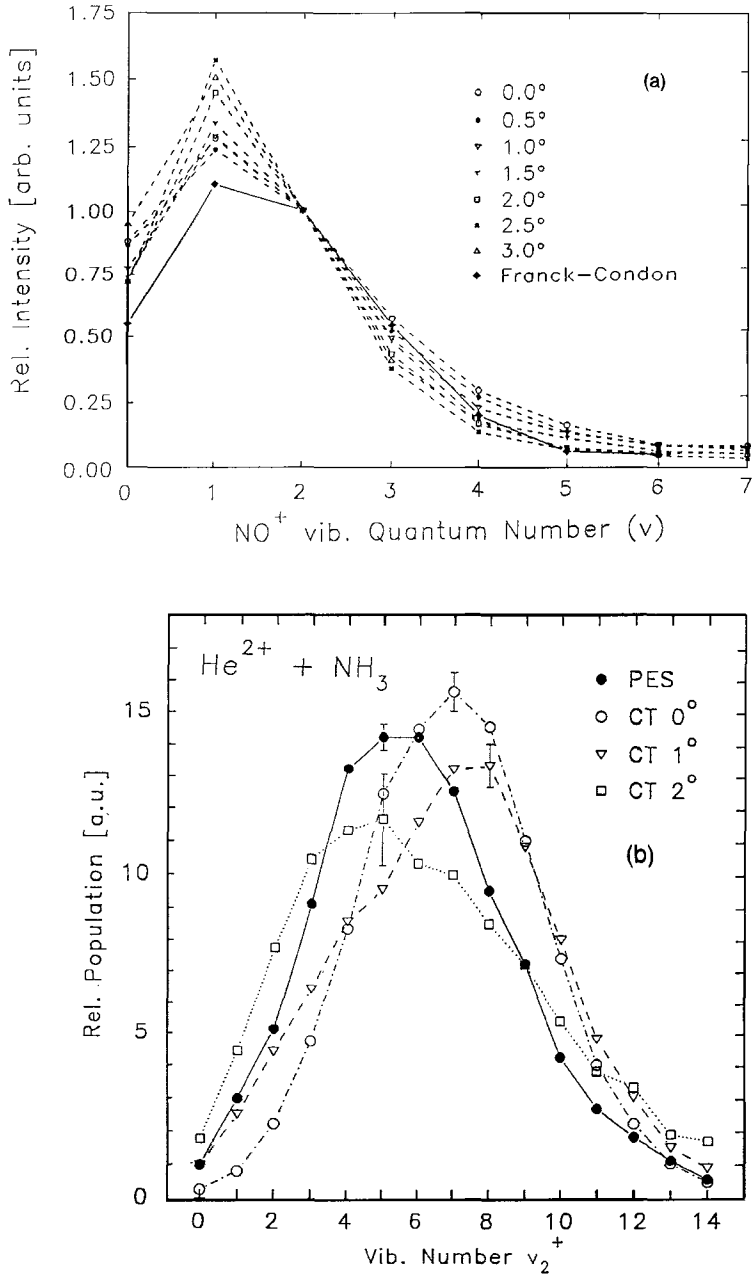

Figure 18. Relative populations of vibrational levels of molecular charge transfer products at indicated laboratory scattering angles (solid points: Franck–Condon factors from photoelectron spectra): (*a*) NO^+ from reaction (10) (Fárník *et al.* 1993); (*b*) NH_3^+ from reaction (11) (Fárník *et al.* 1995).

are shown in figure 17. Figure 18(*a*) summarizes the relative population of the product ion vibrational levels as a function of the scattering angle and also shows a comparison with the respective Franck–Condon (F–C) factors obtained from photoelectron spectra and theoretical calculations. The populations are very similar,

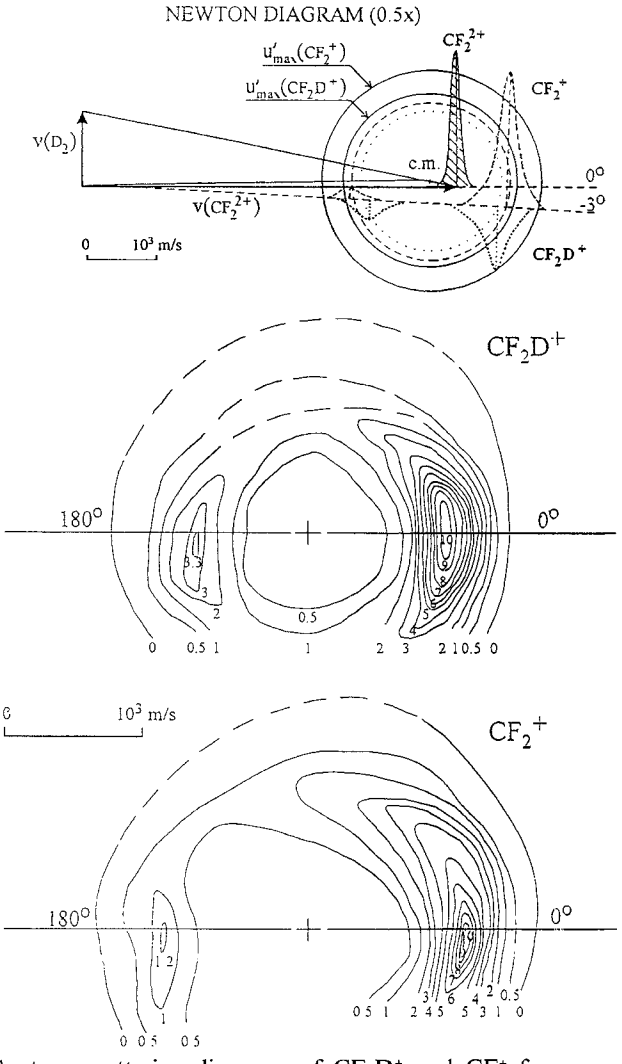

Figure 19. Contour scattering diagrams of CF_2D^+ and CF_2^+ from reaction (12) and (13), respectively; horizontal line shows the direction of the relative velocity vector, cross marks the position of the tip of the c.m. velocity vector. Upper part: the respective Newton diagram with velocity profiles of the reactant and product ions (Dolejšek *et al.* 1995).

and the charge transfer spectra exhibit populations of the lowest levels by about 10% higher than those given by the Franck–Condon factors.

Figure 18(*b*) illustrates results of the population of vibrational levels of NH_3^+ obtained in studies of the charge transfer process (Fárník *et al.* 1995)

$$He^{2+} + NH_3(^1A_1) \rightarrow He^+{}^*(^2P) + NH_3^+(^2A_1, v^+) \quad (\Delta E_{v=0} = 3{\cdot}42\ \text{eV}). \tag{11}$$

The deviation from the Franck–Condon factors was not large and depended on the scattering angle. The reason for the observed differences was discussed by Fárník *et al.* (1995): it might be due to a slight perturbation of the target by the approaching projectile or, possibly, to an increased probability of excitation in the charge transfer spectra of the combination vibrational progression $v_1^+ + nv_2^+$ (or $2v_4^+ + nv_2^+$) which is

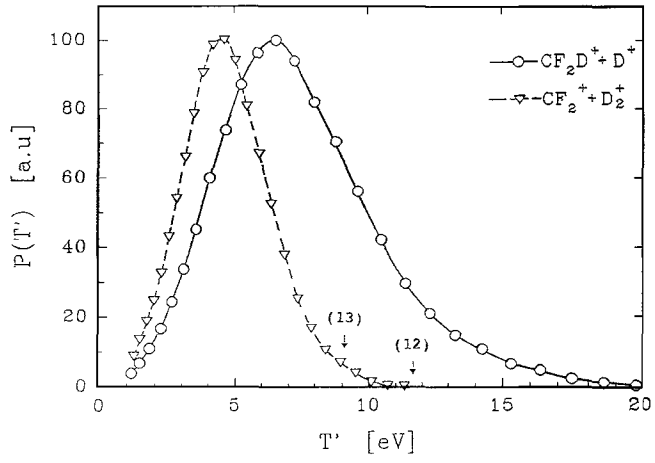

Figure 20. Relative translational energy distributions, $P(T')$, of products of reactions (12) and (13); arrows mark the maximum energy available in the reactions (Dolejšek *et al.* 1995).

known to underline the long bending v_2^+ progression in the ground state of the ammonia ion. In the case of $He^{2+} + H_2S$ charge transfer, the population of the vibrational states of the product molecular ion at the scattering angle 0° was almost the same as given by the Franck–Condon factors ($v_1^+ = 0$ prevailingly populated). At higher scattering angles vibrational levels $v_1^+ = 1, 2, 3$ were populated with a somewhat higher probability than expected from the Franck–Condon factors.

The velocity of the 70 eV projectile in the above mentioned experiments was $5{\cdot}8 \times 10^6$ cm s^{-1} and the average passage time through the regions of crossings was about comparable with a characteristic vibrational frequency; e.g. in the case of ammonia, where the crossings of $v_2^+ = 14$ and $v_2^+ = 0$ occur at R_c of 9 Å and 4·2 Å, respectively, the collision time was $t_{coll} \simeq 1{\cdot}5 \times 10^{-14}$ s, to be compared with the vibrational periods of ammonia bending and symmetric stretching frequencies of $3{\cdot}7 \times 10^{-14}$ s and 1×10^{-14} s, respectively. However, at these collision energies another characteristic transition time t_0 becomes important which is dependent also on the slopes of the crossing diabatic potentials (Child 1974). In our case $t_0 \simeq 1 \times 10^{-15}$ s and one may expect the vibrational state distributions to differ only slightly from the Franck–Condon distributions, as observed.

3.4. *Chemical reactions of dications*

The observation of bond-forming, chemical reactions of dications has been a fairly recent development. The occurrence of chemical processes was briefly mentioned in flow tube studies of Ca^{2+} and Mg^{2+} reactions with simple molecules (Spears *et al.* 1972). A series of bond-forming reactions of transition metal atomic dications (Ti^{2+}, Ta^{2+}) with simple molecules has recently been described (Weisshaar 1993). Both singly- and doubly-charged chemical products containing the transition metal atom were observed. Very recently, the observation of bond-forming reactions of molecular dications such as $CO_2^{2+}, CF_2^{2+}, COS^{2+}$ etc. in collisions with simple molecules, namely D_2, has been reported (Price *et al.* 1994). The bond-forming reactions led to various singly-charged products containing D or D_2 and they were accompanied by charge transfer processes. The remarkable feature of these processes is that the heats of

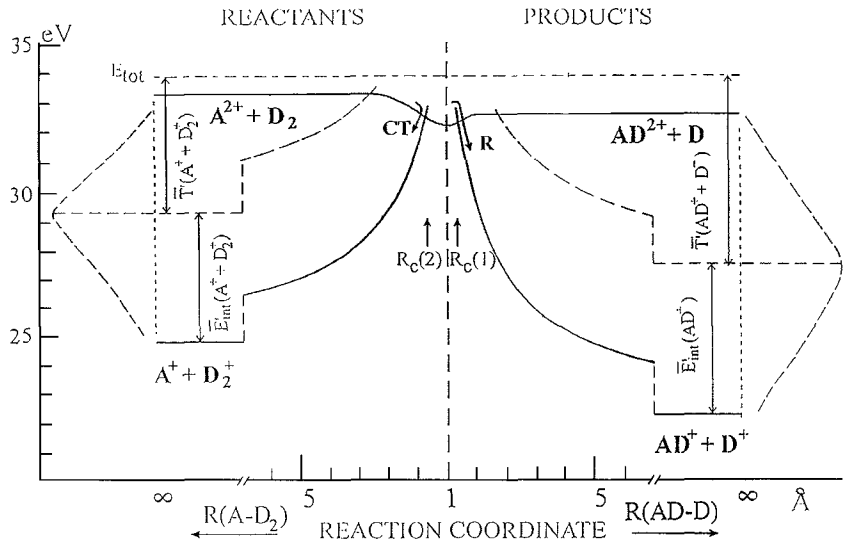

Figure 21. Schematics of a cut through the potential energy surfaces along the reaction coordinate for a dication–molecule chemical and charge transfer reaction (Dolejšek *et al.* 1995).

formation of the dication reactants are very high (above 3000 kJ mol^{-1}). This implies that a large amount of energy, unusually high for chemical reactions, is likely to be interchanged in the bond-forming processes. The question arises of how such a high energy is deposited in the reaction products.

We carried out a beam scattering study on the system $CF_2^{2+} + D_2$ (Dolejšek *et al.* 1995). We were able to identify as the main channels processes

$$CF_2^{2+} + D_2 \rightarrow CF_2D^+ + D^+ \text{ (chemical reaction)} \quad (12)$$

$$CF_2^{2+} + D_2 \rightarrow CF_2^+ + D_2^+ \quad \text{(charge transfer)} \quad (13)$$

Figure 19 shows scattering diagrams of the products CF_2D^+ and CF_2^+ from reactions (12) and (13) obtained at the collision energy $T = 0{\cdot}6$ eV. Both diagrams are remarkably similar and they show the distinct features of the Coulomb repulsion between two products of the same charge. The c.m. angular distributions are rather similar to those obtained in the $Ar^{2+} + He$ charge transfer process at a comparable collision energy. This fact confirms that one can formulate the chemical reaction as written in (12), with D^+ as the second reaction product. It is worth noting that (12) represents a rare case of a chemical process in which a proton is formed. The product relative translational energy distribution, $P(T')$, provide information on partitioning of the energy available in the reaction (figure 20): the distributions show that in the most likely chemical reaction about 6·5 eV goes into relative translational energy of the products and the rest into internal (electronic and/or vibrational) energy of the molecular product; in the charge transfer process about 4 eV goes into relative translation and the rest into internal energy of the products. Very little is known about the electronic states of the fluorinated molecular products and therefore little can be suggested about the internal (electronic versus vibrational) energy partitioning.

The results on studies of the dynamics of reactions (12) and (13) led us to the formulation of a simple model which described the competition of the chemical and

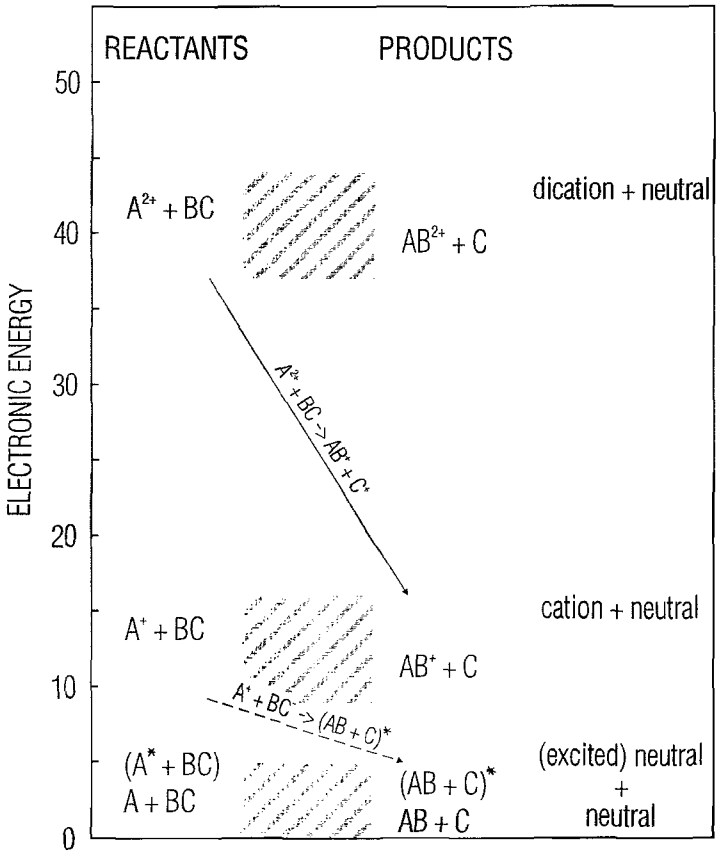

Figure 22. Schematics of chemical reactions of neutrals, cations and dications in the electronic energy scale.

charge transfer processes in a dication–molecule system $A^{2+} + d_2$ (figure 21). Three types of potential energy surfaces are involved:

- slightly attractive potential energy surface(s) of the dication;
- Coulomb repulsive surface(s) of the charge transfer channel $A^+ + D_2^+$;
- Coulomb repulsive surface(s) of the chemical rearrangement channel $AD^+ + D^+$.

The system approaches along a dication surface $A^{2+} + D_2$ in the reactant valley and may make a non-adiabatic transition when crossing with the charge transfer surface(s) forming $A^+ + D_2^+$. Those systems which do not end as charge transfer products continue on the dication surface which presumably has to extend into the product valley in order to cross with the product potential energy surface(s) $AD^+ + D^+$ rising steeply—due to the Coulomb repulsion between the chemical products—from the product valley. Note that large adiabatic splitting of the surfaces at R should facilitate the formation of the chemical products.

The observation of chemical, bond-forming reactions of dications leads to a general view of various classes of chemical reactions of neutrals, cations and dications from the point of view of the electronic energy of reactants and products involved (figure 22). Lowest on the energy scale are reactions of ground state and excited neutrals, where the electronic energy of most reactants and products is about 0–6 eV and

exoergicities of the reactions are about 0–4 eV. Above it there is the energy region of ion–molecule reactions; ionization energies to form most cations are between 9–15 eV and usual exoergicities of ion–molecule processes are again 0–4 eV. Rather higher than this region, at 38–43 eV, there is the energy band of dication–molecule reactions which may lead to dication products of a similar energy content with exoergicities expected to be also a few eV. The neutral–neutral and ion–molecule reactions have been widely investigated, reactions of dications with molecules (leading to a dication product) have been reported. However, of special interest are those types of chemical reactions which *interconnect* these various classes, i.e. elementary chemical processes of changing cations to neutrals or dications to cations. The interconnection between cation–molecule and neutral–neutral reactions is provided, for example, by bond-forming associative recombination reactions of the type $A^+ + BC^- \rightarrow (AB + C)^*$. From the investigation of these processes it is known that most of the energy released goes into internal energy of the product(s). Very interesting and little known is, of course, a connection between dication–molecule and cation–molecule chemical reactions. The results discussed here shed light on the energy interchange in at least one possible type of these processes: those in which two singly-charged ions are formed. The first results show that a considerable part of the huge energy available goes into relative translation (an unusually large part for a chemical process) and the rest goes into internal energy of the products formed. Obviously, it is difficult to make far-reaching conclusions from only the few systems studied and much more work is needed to sufficiently map the field. However, the observation of chemical reactions of dications does appear to open a novel field of interesting chemical processes.

Acknowledgments

This paper is dedicated to Michael J. Henchman as an expression of my respect for his personality, his contribution to studies of ion–molecule collisions, and his deep insight into the problems of this field.

The author would like to express his thanks to the collaborators at the Prague Institute: to former and present graduate students (B. Friedrich, J. Vančura, M. Sadílek, M. Fárník) and to L. Hládek and Z. Dolejšek. Special thanks go to colleagues in the laboratories, where some of the experiments were carried out: to J. H. Beynon and his co-workers P. Jonathan and A. G. Brenton at the Royal Society Research Unit, University College of Swansea, and to J. P. Toennies and his co-workers T. Ruhaltinger and R. G. Wang at the Max-Planck Institute für Strömungsforschung, Göttingen. Financial support for various parts of this research by grants of the Academy of Sciences (Nos. 44013, 440410), of the Grant Agency of the Czech Republic (No. 93/203/0230), and of the EC Network 'Structure and Reactivity of Molecular Ions' is gratefully acknowledged.

The kind permission of Elsevier Science–NL to reprint figures 4–6, 7*a*, 8–11, 14, 17, 18*a*, 19–21 from papers of the author and his co-workers published earlier in *Chem. Phys. Lett.* and in *Int. J. Mass Spectrom. Ion Proc.*, and of the American Institute of Physics to reprint figures 3 and 18*b* from papers in *J. chem. Phys.* is gratefully acknowledged.

References

BRAGA, J. P., KNOWLES, D. B., and MURRELL, J. N., 1986, *Molec. Phys.*, **57**, 665.
CHILD, M. S., 1974, *Molecular Collision Theory* (New York: Academic).

DALGARNO, A., 1985, *Nucl. Instrum. Methods Phys. Res. B*, **9**, 655.
DALGARNO, A., 1993, private communication.
DAWBER, G., MCCONKEY, A. G., AVALDI, L., MACDONALD, M. A., KING, G. C., and HALL, R. I., 1994, *J. Phys.*, **27**, 2191.
DOLEJŠEK, Z., FÁRNÍK, M., and HERMAN, Z., 1995, *Chem. Phys. Lett.* **235**, 99.
DYKE, J. M., GOLOB, L., JONATHAN, N., MORRIS, A. and OKUDA, M., 1974, *J. Chem. Soc. Faraday Trans.* II, **70**, 1828.
FÁRNÍK, M., 1991, *Thesis*, Faculty of Mathematics and Physics, Charles University, Prague.
FÁRNÍK, M., and HERMAN, Z., 1991, unpublished results.
FÁRNÍK, M., HERMAN, Z., RUHALTINGER, T., and TOENNIES, J. P., 1995, *J. chem. Phys.*, **103**, 3495.
FÁRNÍK, M., HERMAN, Z., RUHALTINGER, T., TOENNIES, J. P., and WANG, R. G., 1993, *Chem. Phys. Lett.*, **206**, 376.
FRIEDRICH, B., and HERMAN, Z., 1984a, *Collect. Czech. Chem. Commun.*, **49**, 570.
FRIEDRICH, B., and HERMAN, Z., 1984b, *Chem. Phys. Lett.*, **107**, 375.
FRIEDRICH, B., PICK, Š., HLÁDEK, L., HERMAN, Z., NIKITIN, E. E., REZNIKOV, A. I., and UMANSKII, S. YA., 1986, *J. chem. Phys.*, **84**, 807.
FRIEDRICH, B., VANČURA, J., and HERMAN, Z., 1987, *Int. J. Mass Spectrom. Ion Processes*, **80**, 177.
FRIEDRICH, B., VANČURA, J., SADÍLEK, M., and HERMAN, Z., 1985, *Chem. Phys. Lett.*, **120**, 243.
HAMDAN, M., and BRENTON, A. G., 1989, *J. Phys.* B, **22**, L45.
HANSEL, A., RICHTER, R., LINDINGER, W., and HERMAN, Z., 1992, *Int. J. Mass Spectrom. Ion Processes*, **177**, 213.
HERMAN, Z., JONATHAN, P., BRENTON, A. G., and BEYNON, J. H., 1987, *Chem. Phys. Lett.*, **141**, 433.
JANEV, R. K., and WINTER, H., 1985, *Phys. Rep.*, **117**, 267.
KOBAYASHI, N., NAKAMURA, T., and KANEKO, Y., 1983, *J. Phys. Soc. Jpn.*, **52**, 2684.
LARSSON, M., 1993, *Comments at. mol. Phys.*, **29**, 39.
LARSSON, M., OLSSON, B. J., and SIGRAY, P., 1989, *Chem. Phys.*, **139**, 457.
LENNON, M., MCCULLOUGH, R. W., and GILBODY, H. B., 1983, *J. Phys.* B, **17**, 2191.
MATHUR, D., 1993, *Phys. Rep.*, **225**, 193.
MORGAN, R. P., BEYNON, J. H., BATEMAN, R. H., and GREEN, B. N., 1978, *Int. J. Mass Spectrom. Ion Processes*, **28**, 171.
OKUNO, K., and KANEKO, Y., 1983, *Atomic Collision Res. Jpn.*, **9**, 56.
OLSON, R. E., 1972, *J. chem. Phys.*, **56**, 2979.
PRICE, S. D., MANNING, M., and LEONE, S. R., 1994, *J. Am. chem. Soc.*, **116**, 8673.
SADÍLEK, M., VANČURA, J., FÁRNÍK, M., and HERMAN, Z., 1990, *Int. J. Mass Spectrom. Ion Processes*, **100**, 197.
SATO, Y., and MOORE, J. H., 1979, *Phys. Rev.* A, **19**, 495.
SPEARS, K. G., FEHSENFELD, F. C., MCFARLAND, F., and FERGUSON, E. E., 1972, *J. chem. Phys.*, **56**, 2562.
WEISSHAAR, J. C., 1993, *Accs. chem. Res.*, **26**, 213, and references cited therein.